Fluorescent characterization of vanillin aurone

by

Beth Anderson

A Thesis Submitted in Partial Fulfilment of the Requirements for the Degree of Master of Science in Chemistry

Middle Tennessee State University

March 2022

Thesis Committee:

Dr. Justin M. Miller, Chair

Dr. Andrienne Friedli

Dr. Scott Handy

ACKNOWLEDGEMENTS

Thank you to Dr. Miller for his guidance and mentorship throughout my research experience. I am grateful for all the members of the Miller Lab that have been a family of students that challenge, help, and spur each other on. It has been a joy to be a part of this group for the last two years. Thank you to Dr. Scott Handy, Chad Brambly, and Daniel L. Bryant at Middle Tennessee State University, and Samer Gozem at Georgia State University for their contributions to this work. Finally, thank you to Avraz Anwar for his constant support and encouragement.

ABSTRACT

Since their discovery, fluorescent molecules have been used for a variety of purposes such as fluorescent tags in antibody assays, anterograde tracing in neuroscience studies, production of lasers, fluorescent cell imaging and many other areas. Fluorophores are powerful visualization tools and thus the development of novel, small organic fluorophores is in great demand. One such small organic fluorophore is derived from an aurone, 2-benzylidenebenzofuran-3(2H)-one, a molecule with the general structure of a benzylidene attached to a benzofuran at the second position. An aurone with a methoxy group at the 3' position and a hydroxyl group at the 4' position is termed vanillin aurone after the synthesis of the molecule by addition of vanillin to benzofuranone through an acid catalyzed Aldol condensation.

In this study we evaluate the fluorescent capabilities of the vanillin aurone through a series of fluorescent titrations in various solvent environments assessing it's solvatochromic behavior. Weakly polar, aprotic solvents amplify the fluorescent intensity of the molecule and blue shift the peak emission wavelength. To better understand the solvatochromic trends, extinction coefficients were determined in different solvents. These data point to another explanation for the fluorescent disparities independent of differences in photon absorption efficiency. As computational simulations show a promising interaction between the vanillin aurone and the active site of the ATP binding domain of YME1L AAA+, this protein has been used as a model system supporting vanillin aurone binding to ATPases. This binding to a family of proteins ubiquitous in cells provides an avenue for future, potential therapeutic development.

TABLE OF CONTENTS

LIST OF TABLES AND FIGURES

LIST OF ABBREVIATIONS

AAA+ - ATPases associated with various cellular activities

ADP - adenosine diphosphate

ANOVA – analysis of variance

ATP – adenosine triphosphate

C-PCM – conductor-like polarizable continuum model

DFT – density functional theory

DMSO – dimethyl sulfoxide

EDTA – ethylenediaminetetraacetic acid

EtOH – ethanol

FRET – fluorescence resonance emission transfer

HEPES – N-2-hydroxyethylpiperazine-N'-2-ethanesulfonic acid

IC50 – half maximum inhibitory concentration

LSM – laser scanning microscope

MD – molecular dynamics

NMR – nuclear magnetic resonance

NPT – MD ensemble with substance (N), pressure (P), and temperature (T) held constant

NTP – nucleoside triphosphate

NVT - MD ensemble with substance (N), volume (V), and temperature (T) held constant

PBS – phosphate buffered saline

PDB – protein data bank

RPA – random phase approximation

RPMI – Roswell Park Memorial Institute, growth media

RMSD - root-mean-square-deviation

TD-DFT – time-dependent density functional theory

TICT – twisted intramolecular charge transfer state

T-PMT – transmitted detection module-photomultiplier tube

VEEEs – vertical electronic excitation energies

YME1L-AAA+ - ATP binding domain of YME1L

Fluorescent Characterization of the Vanillin Aurone

CHAPTER 1: INTRODUCTION

1. Fluorescence

Fluorophores, molecules that exhibit fluorescence, have been utilized as tools for scientific study since the discovery of the first synthetic fluorophore, fluorescein, reported by Adolf von Baeyer in 1871.[1] Many other fluorophores have been synthesized since then such as rhodamine, Acridine Orange, and a host of Alexa Fluor dyes. However, there are also natural fluorophores such as the fluorescent amino acids, tryptophan and tyrosine, which contribute to fluorescence-based protein studies. Other natural fluorophores include lignin, chlorophyll, and flavonoids and often contribute to pigmentation in plants.[2]

The experimental applications of fluorophores vary widely from biological immunofluorescent studies to protein dynamics and even laser production. [3-4] Fluorescent spectroscopy is very sensitive, requiring only a small amount of sample or a small concentration of the fluorophore, and therefore, is a beneficial technique for trace analysis.[5] Because organic, fluorescent molecules can be very small in size they are useful for detection in biological assays as well and do not typically interact with the biochemical system being studied.[6] Thus, the synthesis and characterization of novel small, organic fluorophores is in high demand among the scientific community.

2. Aurones

One known family of under-explored fluorophores are aurones. Aurones, are a subclass of flavones that have a yellow-golden color and are found in many

flowers, fruits, and vegetables where they contribute to pigmentation. [7] Their structure consists of a benzylidene substituent attached to a benzofuran ring at the 2 position (**figure 1**). Aurones are natural products that have been of interest to the scientific community as potential therapeutics. They have shown promise as antiparasitic, antifungal, and antioxidants. [8-10]

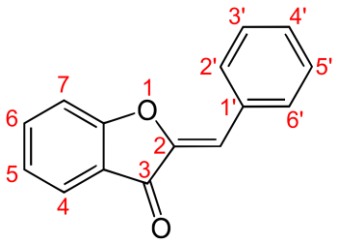

Figure 1 General structure of an aurone with numbering scheme

Less studied is the fluorescent capability of these aurones. As they contain a conjugated ring system and are small in size relative to common synthetic options. Aurones provide a promising fluorescent skeleton that can be enhanced by the addition of a range of substitutions. Optimization of aurone fluorescence could lead to the development of biologically relevant fluorescent dyes, probes, and chemo sensors.[11]

Some work has been done to evaluate the effect of derivatization of the aurone structure on fluorescence emissions. Shanker *et al.* who synthesized four 4'-Aminoaurones observed red shifted absorbance and emission spectra due to the addition of electron rich groups on the benzene.[12] Solvatochromic trends were observed as solvent polarity increased, fluorescence intensity decreased, and emission wavelengths were red shifted. They also showed that their aurone

derivatives are cell permeable such that they were able to use them as fluorescent cell dyes. The addition of halide, hydroxyl, and methyl substituents at various positions on the benzofuran ring was explored by the Handy lab. They found that when halogens were added closer to the carbonyl, at positions 4 and 5, absorbance spectra were red shifted. Toxicity studies also revealed that methoxy and hydroxy substituted compounds were more toxic that the only halide substituted derivatives. [13] The addition of bromine and methyl groups at positions on both the benzene and the benzofuran was reported by Espinosa-Bustos and colleagues. They observed that across the board, aurones in less polar solvents displayed increasingly wider Stokes shifts as well as increased in fluorescent intensities.[11] Because distinct solvatochromic behavior is observed consistently regardless of the specific derivatization, this is an important characteristic that can be manipulated in studies utilizing aurone fluorescence. Based on previous work, we expect that vanillin aurone derivatives yield brighter and more blue shifted fluorescence when in will less polar solvents environments, as is consistent with the work of Espinosa-Bustos and coworkers as well as Shanker and coworkers.

3. Vanillin aurone

The vanillin aurone is an aurone derivative in which the benzene ring has been replaced with vanillin, such that there is now a methoxy group at the 3' position and a hydroxyl group at the 4' position. (**figure 2**) This addition of electron donating groups contributes to the delocalized electrons involved in the fluorescence process and thus increases fluorescent intensity.

Here we report that vanillin aurone excites between 418-436 nm and shows maximum emissions between 490-540 nm depending on the solvent condition. The aurone displays strong solvatochromic fluorescent emissions such that an increase in fluorescent intensity is observed as polarity decreases. We asked

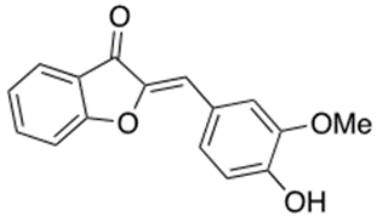

Figure 2: Chemical structure of vanillin aurone

whether vanillin aurone could be a useful small molecule fluorophore with unique advantages due to its specific solvent sensitivities. We characterize the vanillin aurone's fluorescent properties and investigate broader applications of the dye in biochemical assays as well as evaluate its limitations. In order to assess the solvatochromic behavior of the dye, emissions behavior and extinction coefficient calculations were performed in five solvents of systematically varied polarities. Our knowledge of the solvent impact on fluorescence is further informed by time-dependent density functional theory analysis (TD-DFT) done using the five solvents' dielectric constants to determine calculated values for fluorescence characteristics. These data alongside the experimental data supports the conclusion that vanillin aurone emits from a heterogeneous mixture of three fluorescent excited states: planar, twisted intermolecular charge transfer state, and deprotonated. We see that the solvent environment likely influences the majority fluorescent state from which the excited vanillin aurone emits.

Our computational data suggest that emissions largely result from a planar excited state. For this reason, we next performed studies to determine whether protein binding could promote altered emissions due to altered conformation. We explore the binding potential of vanillin aurone to the model AAA+ binding domain of YME1L. Vanillin aurone-stained HeLa cells were imaged by fluorescence microscopy to show cell membrane permeation. Taken together, these results indicate that the vanillin aurone could be useful as a starting point for future therapeutics targeting nucleotide hydrolase.

CHAPTER 2: RESULTS AND DISCUSSION

1. Solvatochromic behavior

To characterize vanillin aurone fluorescence, titrations were performed wherein vanillin aurone concentration was systematically increased in solvents ranging in polarity from low to high. By doing this we hoped to define fundamental photo physical parameters including λ_{ex}, λ_{max}, Stokes shift, and linear range of detection as a function of solvent. The five solvents used throughout this work are dimethyl sulfoxide (DMSO), H_2O, ethanol, acetone, and toluene. For these fluorescent titrations an optimal excitation wavelength was determined for each solvent condition first by executing an excitation scan of vanillin aurone in solution. In the excitation scan, emissions are observed at a fixed wavelength while the excitation wavelength is varied. The wavelength yielding maximum emissions can be inferred to reflect the wavelength supporting maximum absorbance. As **figure 3.A** shows, the largest excitation wavelength is found in the water

condition at 436 nm and the smallest at 418 nm for the acetone condition. Even still, absorbance wavelengths of the vanillin aurone do not appear to vary greatly and stay roughly within the range of 420 nm to 440 nm. The fluorophore displays large Stokes shifts in all solvent conditions with the largest gap seen in the H_2O solvent condition at 103 nm. As seen in the table in **figure 3.A,** which indicates the polar nature of each solvent used alongside the observed Stokes shift of vanillin aurone, the Stokes shifts increase as the polarity of the solvent increases. Protic nature was also highlighted here as we speculate that the observed solvent

A)

Solvent	Relative Polarity	Protic or Aprotic	Abs (nm)	Emission (nm)	Stokes Shift (nm)
Toluene	0.099	A	423	491	81
Acetone	0.355	A	418	499	93
DMSO	0.444	A	421	514	91
EtOH	0.654	P	425	516	68
H_2O	1	P	436	539	103

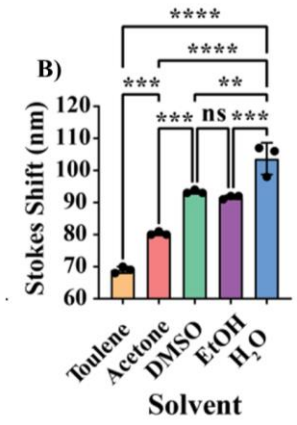

Figure 3: Comparative solvent effects. all data was obtained by triplicate fluorescent titrations in each solvent environment. **A)** table of absorbance or excitation wavelengths, emission wavelengths and the calculated Stokes shift for vanillin aurone in each solvent environment shown alongside extended information about the nature of each solvent used, including relative polarity and protic character. [14] **B)** graphical representation of Stokes shift trend. Solvents are organized by increasing polarity from left to right. These data were treated with one way ANOVA analysis and pairwise comparisons are included above the data points to indicated significant variance. **ns =** not significant with a p> 0.1234, ********p < 0.0001, *******p < 0.0002, ******p < 0.0021, *****p < 0.0332

dependent trends are due to hydrogen bonding with the hydroxyl group of the vanillin ring. This intermolecular interaction impacts fluorescence by diminishing the overall emission intensity. **Figure 3.B** depicts this trend graphically as the solvents are arranged in order of increasing polarity from left to right.

Besides the Stokes shift, other spectral differences are observed as a result of the solvent environment such as varying fluorescence intensity and maximum emission wavelength. We observe that as polarity of the solvent increases, fluorescence intensity is hypochromic, that is fluorescence intensity decreases (**figure 4**). With that trend we might expect to observe hyperchromic, or increased, fluorescence intensity of vanillin aurone in toluene. However, when in the nonpolar environment of toluene, fluorescence emissions are relatively low showing an intensity of roughly 6 hundredths of the fluorescence emissions observed in acetone. We speculate that this low fluorescence could be a result of potential pi-pi stacking between toluene and the benzofuran ring of vanillin aurone resulting in fluorescence quenching. In **figure 4.A** the linear increase in maximum fluorescence intensity is plotted as a function of increasing fluorophore concentration and we see that the polar solvent H_2O shows dramatically lower fluorescence intensities as compared to the more weakly polar solvents like DMSO. The solvent environments which yielded the greatest fluorescence emissions, acetone and DMSO, show fluorescent signals that begin to deviate from linearity at higher vanillin aurone concentrations. This deviation indicates an upper limit to the linear range of detection for vanillin aurone in these solvents which is important to be aware of for use of vanillin aurone signal for quantitative purposes.

Figure 4.B overlays the fluorescent spectra of vanillin aurone in each solvent condition. It is observed here and further pointed out in the table in **figure 4.C** that with increasing polarity of the solvent environment vanillin aurone fluorescence in quenched. This is supported by the near negligible fluorescence observed in the H_2O condition. Vanillin aurone in ethanol was more weakly

fluorescent, showing intensities roughly four times lower than those observed in acetone, an observation consistent with the hypothesis that a protic solvent

A)

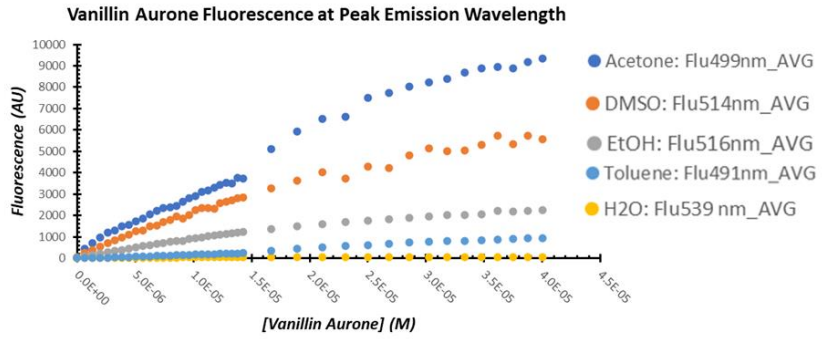

B)

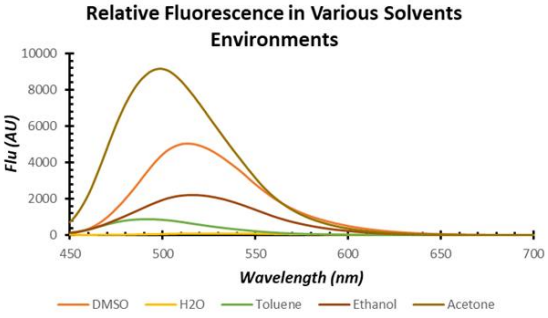

C)

Solvent	Polarity Index	Maximum Emission Wavelength (nm)
Toluene	0.099	491
Acetone	0.355	499
DMSO	0.444	514
EtOH	0.654	516
H_2O	1	539

Figure 4: Solvent effects on fluorescent emissions. A) Each data point represents an average of data collected in triplicate. Fluorescent intensities are plotted as a function of vanillin aurone concentration. The figure legend identifies the solvents used as well as the maximum emission wavelength of vanillin aurone in each solvent. The fluorescent intensities graphed here are the intensities of vanillin aurone at those specified wavelength for each fluorophore concentration. **B)** Each line is the average spectra of three replicates of fluorescence collected in each specified solvent, labeled in figure legend, and shows 40 μM vanillin aurone fluorescence as a function of wavelength. **C)** The impact of solvent polarity is highlighted as the polarity index is tabulated alongside the maximum emission wavelength for each of the five solvents.[14]

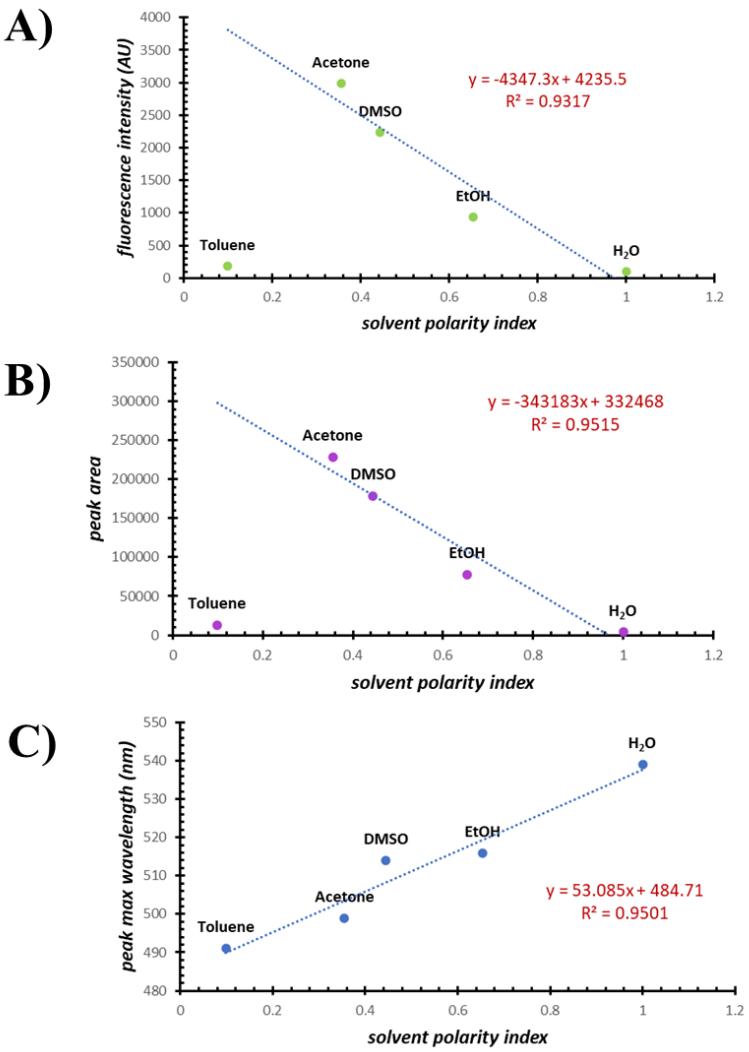

Figure 5: Impact of solvent polarity on fluorescence. All data points are averages from titration experiments conducted in triplicate. For these data 10.18 μM vanillin aurone was used. **A)** Fluorescent intensity of vanillin aurone is plotted as a function of the solvent polarity index and each data point is labeled with the corresponding solvent environment.[14] Excluding the Toluene condition, these data were fit with a linear regression and the resultant line is printed on the graph along with the r^2 value. **B)** Peak area is plotted as a function of the solvent polarity index with the solvent condition for each data point labeled above. Excluding the toluene solvent condition, these data were fit to a linear regression with the resultant line printed on the graph along with the r^2 value. **C)** Peak wavelength in nm is plotted as a function of the solvent polarity index with the solvent condition for each data point labeled above. All data points were fit to a linear regression and the resultant line is printed on the graph along with the r^2 value.

environment negatively impacts the fluorescent capability of vanillin aurone. As shown in **figure 4.c**, as polarity of the solvent increases, the maximum emission wavelength is red shifted.

To cumulatively reflect on the observed solvent effects, we considered relative solvent polarity and the specific impact this property has on vanillin aurone fluorescence. Though the nonpolar solvent toluene correlates with very low fluorescence, the more weakly polar solvents seem to facilitate large fluorescent emissions. When plotted as a function of solvent polarity index, fluorescence intensity decreases linearly for polar solvent conditions (**figure 5.A).** These data were fit with linear least squares regression producing an equation in the form of $y = mx + b$ where m=-4347.3, b=4235.5, and $r^2 = 0.9317$. Peak area, that is the area under the curve, shows a similar trend decreasing as the solvent environment becomes increasingly polar (**figure 5.B**). The equation that resulted from the linear fit of these data is in the form of $y = mx + b$ where m=-343,183, b=332,468, and $r^2=0.9515$. For both the fluorescence intensity and the peak area trend, we excluded the toluene condition from the linear fit as it is an outlier in both data sets. As previously mentioned, we speculate that toluene engages in pi-pi stacking interactions with the vanillin aurone rings giving rise to this deviation from linearity in the fluorescence intensity and peak area trends. Though previously determined that peak emission wavelength is red shifted as a result of increased solvent polarity, when plotted as a function of solvent polarity index we see that

this decrease is linear yielding an equation of best fit with the form y = mx + b where m=53.085, b=484.71, and the r^2 value is 0.95 (**figure 5.C**).

As the expression of solvatochromic behavior is common among chromophores, it was not surprising to observe such trends in vanillin aurone fluorescence. Upon absorption of a photon, the electrons in a fluorescent molecule rearrange, intensifying the dipole moment. In response to this excited state, the surrounding solvent molecules must reorganize around the fluorophore.[5] This phenomenon is the basis for the nonspecific solvent sensitivity expressed by all fluorophores. However, solvent sensitivity that arises from specific solvent-fluorophore interactions, such as hydrogen bonding, acid-base chemistry, or formation of a solvent-fluorophore complex, more typically lead to significant, distinct spectral shifts. For example, Su *et al* show that intermolecular hydrogen bonding between methanol solvent and hydroxyl substituents on benzaldehyde enhance fluorescent emissions.[15]

2. Impact of the absorbance process on solvatochromism

As increased polarity of the solvent environment leads to an apparent decrease in vanillin aurone fluorescence, we determined the extinction coefficient (ε) of vanillin aurone in each solvent. If the decrease in fluorescence can be attributed to decreased efficiency of the absorption process, vanillin aurone would yield lower ε values for more polar solvent conditions. We determined the ε of vanillin aurone in various solvents by collecting absorbance values for known concentrations of vanillin aurone in each solvent and plotting those absorbances as a function of vanillin aurone concentration. This concentration range was chosen due to

deviation from linearity at higher concentrations. These data were fit with linear least squares analysis producing a line in the form of y = mx +b. This line fits the form of the Beer-Lambert equation.

Equation (1) $$\mathbf{A = bc\epsilon} \quad \mathbf{(1)}$$

Where **A** is absorbance, **b** is the path length, **c** represents the fluorophore concentration, and $\boldsymbol{\varepsilon}$ is the extinction coefficient of vanillin aurone in the specified solvent.[16] When the data is fit to a line with the form of y = mx + b, (y) represents the measured absorbance values, (x) is the known vanillin aurone concentration, and the pathlength (b) is one. Therefore, the only remaining variable, the extinction coefficient, is represented in the resulting equation by the term (m), the slope of the line. The best fit lines produced from these experiments include a y intercept term which ideally would equal zero as there is no y intercept term in the Beer-Lambert equation **(1)**. In this case the y intercepts are a product of some experimental error or background noise, though are still relatively small.

Though we did observe some decrease in the $\boldsymbol{\varepsilon}$ as solvent polarity increased (see **figure 6**), the magnitude of this trend indicates that there is likely another explanation for the decrease in fluorescence. Differences in the extinction coefficient alone do not explain observed differences in emissions occurring in varied solvent systems. The rationale for this statement is drawn from comparison of acetone with ethanol or H_2O, where these solvents share a statistically identical molar extinction coefficient, (see **figure S1**) yet exhibit unique emission

behaviors. It cannot be ruled out that the increased molar extinction coefficient for the vanillin aurone determined in DMSO versus other solvents contributes to the observed solvatochromic behavior. However, the ~2-fold increase in molar extinction coefficient recorded for vanillin aurone in DMSO versus acetone does not account for the increased emission in the latter solvent relative to the former. For these reasons, we predict an alternative mechanism beyond solvent-dependent differences in absorbance properties to explain differences in emission behaviors reported here.

A)

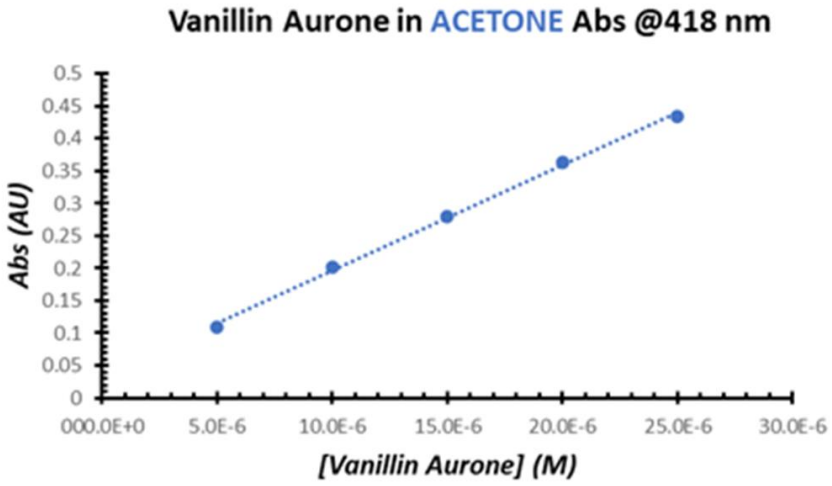

B)

Solvent	Extinction Coefficient ($M^{-1}cm^{-1}$)	Standard Deviation ($M^{-1}cm^{-1}$)
H_2O	14,914	± 486.47
DMSO	25,971	± 922.73
Acetone	16,250	± 1865.94
EtOH	15,780	± 1532.45
Toluene	5,127	± 292.8

Figure 6: **Extinction coefficients for vanillin aurone in different solvents. A)** Representative plot of vanillin aurone absorbance values in acetone as a function of concentration**.** All data points are averages of values collected in triplicate. The data set is fit to a line with the form of y = mx+b where m = 16,250 and b = 0.0339 and an r^2 value of 0.9981. According to the Beer-Lambert law, where A = bcε, the slope of each line is the extinction coefficient (ε) for vanillin aurone in the specified solvent.[16] Data for the other four solvent conditions can be found in **figure S2. B)** For efficient comparison, the extinction coefficients of vanillin aurone in the selected solvent environments are tabulated alongside the calculated standard deviation values for each ε.

4. Computational explanations of solvatochromism

Theoretical calculations done by a collaborator at Georgia State, Dr. Samer Gozem, revealed that there are multiple potential fluorescent states from which the excited electrons in the aurone can relax. The general structure of the vanillin aurone is that of a benzofuran ring connected to the vanillin ring (see **figure 1**). The exocyclic bond between the vanillin and the benzofuran is flexible and, if the molecule is not stabilized by intermolecular interactions, could allow twisting of the molecule out of an otherwise planar structure. In such a twisted state, an intramolecular charge transfer mode of fluorescence is promoted. This structure will be referred to as the twisted intermolecular charge transfer state (TICT) (**figure 7.A**). Another possible fluorescent mode is the planar structure, modeled in **figure 7.B**, where there is no twisting along the exocyclic bond and both the benzofuran and the vanillin rings exist within the same plane. This planar structure is expected to be yield brighter fluorescence than the TICT state as the planar state maintains the extended π network across both ring systems in the vanillin aurone. In the TICT state the twisting around the exocyclic bond disrupts the sharing of pi electrons across the molecule.

As Phenols are known photoacids, in which pKa lowers from roughly 10 to 4 when excited.[17] Thus, the vanillin aurone may convert to a deprotonated state upon excitation. This deprotonated state could arise from either the TICT structure or the planar structure when the hydroxyl group on the vanillin ring is deprotonated (**figure 7.C**).

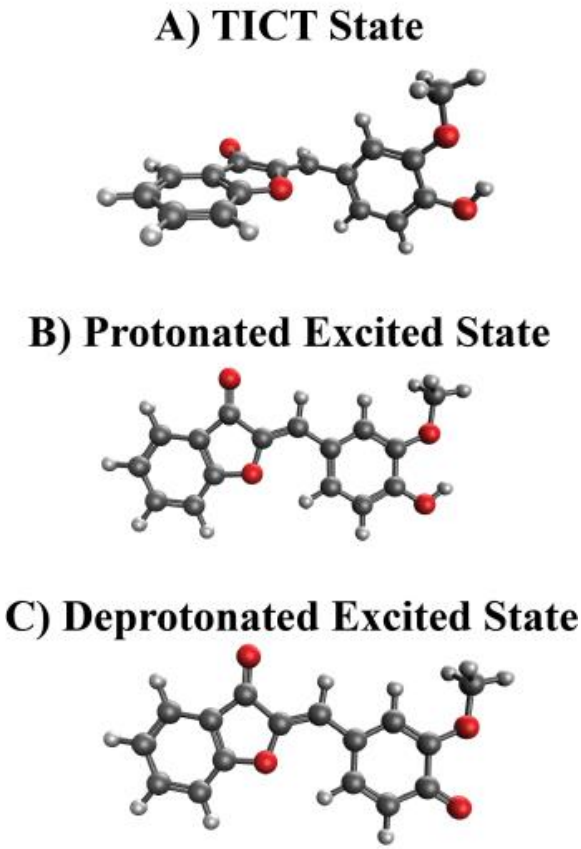

Figure 7: Visual representation of proposed vanillin aurone fluorescent excited states. A) Ball-and-stick model of the planar fluorescent excited state in which both the benzofuran ring and the vanillin ring of the aurone exist within one plane. **B)** Deprotonated fluorescent excited state in which the hydroxyl group on the vanillin ring is deprotonated. The model shown here is in a planar state, however, the hydroxyl group can be deprotonated in either a planar or twisted vanillin aurone structure. **C)** TICT, or twisted intermolecular charge transfer, state in which the vanillin and benzofuran rings are twisted around the exocyclic bond such that the two rings do not reside in the same plane.

A)

Absorbance (nm)			
	Dielectric	Abs_{cal}	Abs_{exp}
Toluene	2.3741	420	423
Acetone	20.493	425	418
Ethanol	24.852	426	421
DMSO	46.826	429	425
Water	78.39	425	436

B)

Emissions WL (nm)					
	Dielectric	Planar	TICT	Deprotonated	Experimental
Toluene	2.3741	459	560	605	491
Acetone	20.493	462	592	553	499
Ethanol	24.852	462	592	552	514
DMSO	46.826	467	594	558	516
Water	78.39	462	595	546	539

Figure 8: Calculated absorbance and emission values alongside experimental. Values calculated by density functional theory for vanillin aurone in the planar, TICT, and deprotonated excited states are tabulated alongside experimental data for each of the five solvent conditions. Note that though a deprotonated TICT is likely to exist, these calculations represent a TICT state that is protonated. **A)** Calculated and experimental absorbance wavelengths are shown alongside the dielectric constant for each solvent. **B)** Calculated and experimental emission wavelengths are shown alongside the dielectric constant for each solvent.

Time dependent density functional theory was applied to each of the three proposed fluorescence excited states, and as shown by our calculations (**figure 8** and **9**), each of these fluorescent states yield different emission trends resulting in variable Stokes shifts. These calculations were conducted using the dielectric constants of each of the five solvents used for the fluorescence titration

experiments, so that the calculated data would reflect the impact of solvent fluorophore interactions. As previously mentioned, a deprotonated state may arise from a planar or a TICT structure. However, TD-DFT calculations were only performed for the deprotonated planar state because the TICT structure is expected to disrupt the conjugated pi system. This would inhibit fluorescence such that any amplification of fluorescence due to deprotonation would be masked by the disruption of the extended pi system.

As shown in **figure 8.A**, the calculated absorbance wavelengths do not vary significantly among the solvent conditions and are in good agreement with the experimental data. This finding is consistent with the experimental extinction coefficients for the vanillin aurone in each solvent condition which were found to be minimally affected by the change in environment. We see generally increased emission wavelengths in the calculated data sets for both the TICT and deprotonated fluorescent states as compared to the planar fluorescent state (**figure 8.B**). These larger emission wavelengths serve to increase the calculated Stokes shift of the TICT and the deprotonated fluorescent states above that of the experimental data (**figure 9.A**). The oscillator strength, which indicates relative fluorescent intensity, does not vary notably in response to the solvent environment. However, the TICT state correlates with significant fluorescent quenching while the largest fluorescent intensities are calculated for the deprotonated state (**figure 9.B**).

A)

Stokes Shift (nm)					
	Dielectric	Planar	TICT	Deprotonated	Experimental
Toluene	2.3741	39	140	185	68
Acetone	20.493	37	167	128	81
Ethanol	24.852	36	166	126	93
DMSO	46.826	38	165	129	91
Water	78.39	37	170	121	103

B)

Fluorescent Intensity					
		Oscillator strength			Relative Intensity
	Dielectric	Planar	TICT	Deprotonated	Experimental
Toluene	2.3741	0.6586	0.0002	0.7938	0.058
Acetone	20.493	0.675	0.0002	0.8253	1
Ethanol	24.852	0.6774	0.0002	0.8254	0.767
DMSO	46.826	0.7076	0.0002	0.8647	0.324
Water	78.39	0.6726	0.0002	0.8227	0.012

Figure 9: Calculated Stokes shifts and fluorescent intensity alongside experimental. Values calculated by density functional theory for vanillin aurone in the planar, TICT, and deprotonated excited states are tabulated alongside experimental data for each of the five solvent conditions. Note that though a deprotonated TICT is likely to exist, these calculations represent a TICT state that is protonated. **A)** Calculated and experimental Stokes shift values are recorded alongside the dielectric constant for each solvent. **B)** Calculated oscillator strength for the vanillin aurone in each of the three fluorescent states is tabulated alongside the dielectric constant for each solvent. The relative fluorescent intensity of vanillin aurone in each solvent environment is reported for comparison.

These calculated data, taken with our experimental data, seem to suggest that the observed fluorescent emissions of the vanillin aurone arise from a heterogeneous mixture of the three possible excited states: planar, TICT, and deprotonated fluorescent states. In such a mixture, fluorescent emissions from the planar deprotonated state and, to a lesser extent, from the planar protonated state would contribute positively to the total observed fluorescent emissions. Emissions from the TICT state contribute negatively and ultimately decrease the overall fluorescent emissions as illustrated by **figure 10**. The relative composition of the heterogenous mixture of fluorescent states is impacted by the solvent environment. Thus, we see varied emissions wavelengths and Stokes shifts among

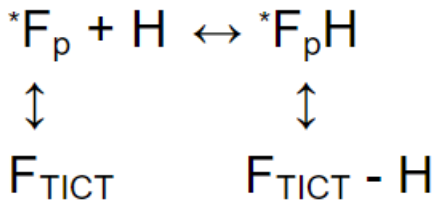

Figure 10: Fluorescent state interconversions. Visual representation of vanillin aurone's transitions from one fluorescent state to another as is expected in a heterogeneous mixture of fluorescent states. $^{*}F_p$ represents the deprotonated planar state. $^{*}F_pH$ indicates the protonated planar state. F_{TICT} and F_{TICT} – H are the twisted intermolecular charge transfer states when deprotonated and protonated respectively.

our experimental data due to shifting equilibria between states. Based on these data, we hypothesize that in a strongly polar environment the vanillin aurone emits from the TICT state more so than in a weakly polar solvent environment.

The interpretation that deprotonation of the hydroxyl group on the vanillin ring contributes to a significant increase in fluorescent emissions is supported by the comparative fluorescence of the piperanol aurone. When modified such that the

vanillin aurone is further cyclized and the hydroxyl is connected to the methoxy group at the 4' position (see structure in **figure S3.A**), forming a piperanol aurone, the possibility of deprotonation is eliminated. The piperanol aurone shows quenched fluorescence like that of the vanillin aurone in water (**figures S3.B and S3.C**) Further experimentation will be necessary to elucidate the factors determining the fluorescent state that vanillin aurone adopts.

4. Vanillin aurone interactions with YME1L-AAA+

4.1. Introduction

As we saw that solvent environment causes a shift in the population of vanillin aurone in a particular fluorescent state, we speculated that binding to a protein could provide a similar environmental shift impacting vanillin aurone fluorescence. As shown in the fluorescent titrations, vanillin aurone is very weakly fluorescent in H_2O, indicating that the polar environment promotes the adoption of a TICT fluorescent state. However, when bound to protein in an aqueous environment we hypothesize that fluorescence will increase as binding provides a more nonpolar local environment around the vanillin aurone or stabilizes the brighter, planar or planar deprotonated fluorescent state. To test this hypothesis, we use a nucleotide binding protein, YME1L, as a model system due to common structural features shared between vanillin aurone and nucleotides.

4.2. YME1L-AAA+ as a model protein

Proteins that couple chemical energy derived from hydrolysis of nucleoside triphosphates (NTPs) to another catalytic activity resulting in the production of mechanical force are frequently referred to as molecular machines or molecular

motors. Such proteins are ubiquitous within the cell and contribute to a diverse range of operations including muscle contraction, cellular transport, and reading and writing genetic material.[18] Among this group of essential proteins is the AAA+ superfamily of ATPases, that is ATPases associated with various cellular activities.[19] Proteins in this superfamily catalyze the hydrolysis of adenosine triphosphate (ATP) often functioning at the interface of two protein subunits. The AAA+ superfamily maintains highly conserved structural features and overall ATP hydrolysis mechanism.

As such, the ATP dependent, inner mitochondrial membrane protease, YME1L, has been shown to be a useful model system for studying the function of AAA+ superfamily proteins. YME1L is a hexameric ATP-dependent protease that is embedded into the inner mitochondrial membrane and contributes to mitochondria morphology and protein quality control. As in other AAA+ protein structures, YME1L structure includes such canonical motifs as the Walker A, Walker B, and P-loop which are integral for ATP binding and hydrolysis.[20] As shown by the work of the Miller lab, the isolated AAA+ binding domain of YME1L (YME1L-AAA+), which purifies as a monomer, is useful as a model for evaluating nucleotide binding of the overall hexameric structure. They show, by way of a series of fluorescent titrations, that YME1L-AAA+ binds ATP and ADP with apparent dissociation constants of 29.11 ± 3.12 μM and 5.5 ± 0.6 μM respectively.[21] Binding of substrate to YME1L-AAA+ is observed through a change in fluorescent signal that is attributed to the altered microenvironment around the fluorescent tryptophan residue, W518, located in the lid domain of YME1L directly adjacent to

the nucleotide binding site (see **figure 11**). As such, when nucleotide is bound, the fluorescent emissions of W518 blue shift from 349 nm to 343 nm. In this way, binding activities can be observed and evaluated with confidence as there is only one intrinsic fluorophore present in the YME1L-AAA+ domain.[19]

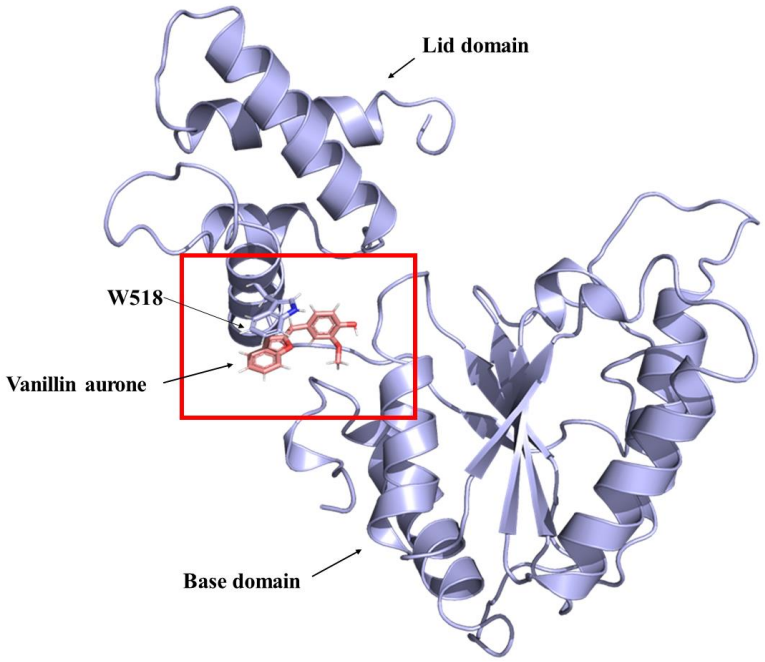

Figure 11: Vanillin aurone docked to YME1L-AAA+. Image of the YME1L-AAA+ domain with vanillin aurone, colored in red, docked within the hinge region of YME1L-AAA+ between the lid and base domains of the protein (red box). W518 is also highlighted in this structure to show the likely pi-pi stacking interaction with the benzofuran ring of vanillin aurone.

4.2. Ligand docking to YME1L-AAA+ domain

The outlined methodology had been used to observe YME1L-AAA+ nucleotide binding, we considered that the structure of vanillin aurone is similar to nucleotide structures in that they both have conjugated ring systems which allow for pi-pi stacking interactions with the indole of Trp residues. For this reason, we

hypothesized that YME1L would be able to bind vanillin aurone as well. If taken as a model system for AAA+ superfamily, it implies the ability of AAA+ superfamily proteins to bind vanillin aurone.

To further explore this potential binding activity, in silico prediction of the interactions of vanillin aurone with the nucleotide binding site of YME1L-AAA+ was conducted by Chad Brambly using rigid body docking coupled to molecular dynamics-based equilibration. It was found that the vanillin aurone docks at the hinge region between the two protein subdomains and is positioned such that the benzofuran rings align in parallel with the indole side chain of the W518 residue (**figure 11**). This suggests that there are pi-pi stacking interactions between the vanillin aurone and the indole of W518. However, these interactions do not seem to change the nitrogen hydrogen bonding of the indole, which predicts that the peak emission wavelength of W518 will not change. Taken together, this work supports the hypothesis that AAA+ proteins are capable of binding vanillin aurone and, upon such a binding event, a shift in fluorescence of the binding site tryptophan should be evident.

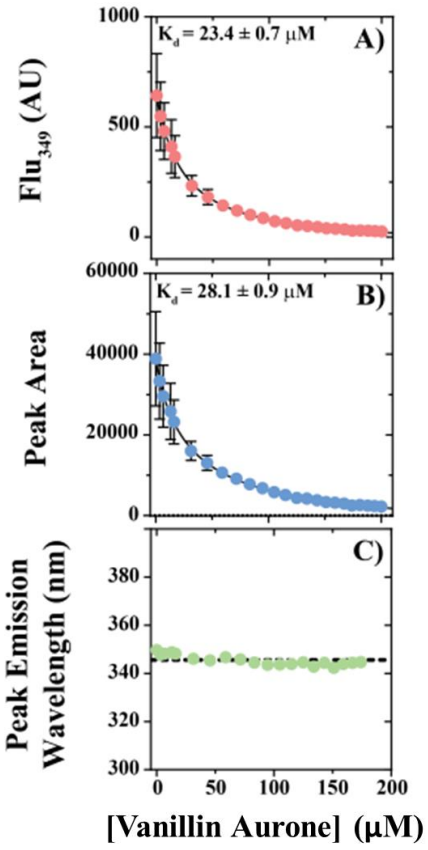

Figure 12: Binding observed through Trp signal All data points and spectral lines shown represent an average of data collected in triplicate **A)** Tryptophan fluorescence is plotted as a function of vanillin aurone concentration. Tryptophan was excited at 295 nm and emissions observed at 349 nm. The straight line is the best fit to the Hill equation with an n constrained to 1 and the resultant parameters are as described in the text. **B)** The area under the curve was calculated for each vanillin aurone concentration and plotted as a function of increasing vanillin aurone concentration. The straight line is the best fit to the Hill equation with n constrained to 1 and the K_d was determined, and other parameters are as described in the text. **C)** The maximum emission wavelength, or peak wavelength, is plotted as a function of increasing vanillin aurone concentration. The dotted black line represents the average value of the data set.

4.3. Binding observed through tryptophan fluorescence signal

With this data in mind, we designed a set of fluorescent titration experiments to evaluate vanillin aurone binding. To observe binding through the perspective of tryptophan fluorescence we conducted a titration in which the protein concentration is held constant and vanillin aurone is added to solution (**figure 12**). Based on the known fluorescent behavior of tryptophan and its high level of solvent sensitivity, the tryptophan signal is expected to decrease upon substrate binding due to the expected pi-pi stacking interaction between the indole of W518 and vanillin aurone. We see that the fluorescence emissions, observed at

349 nm, do decrease with each addition of vanillin aurone as does the peak area. The hyperbolic shape of the graphs suggests that the binding is non-cooperative, and likely, that vanillin aurone and YME1L-AAA+ bind in a 1:1 stoichiometric ratio. (**figure 12.A** and **12.B**)

However, to assess the possibility of multiple vanillin aurone molecules binding to YME1L-AAA+, we fit both data sets to an unconstrained Hill equation. Based on the model that

Equation (2)

$$\mathbf{E + nX \overset{K_{app}}{\rightleftharpoons} EX^n} \qquad \mathbf{(2)}$$

Where **E** is YME1L-AAA+, **X** is the vanillin aurone, **EX** represents the vanillin bound to YME1L-AAA+, and **n** is the Hill coefficient, a term that correlates with the cooperativity of binding.

Equation (3)

$$\mathbf{signal = \frac{A*K_{app}[X]^n}{1 + K_{app}[X]^n}} \qquad \mathbf{(3)}$$

The K_{app} calculated in this way is the inverse of the apparent dissociation equilibrium constant (K_d).[22] From this fit we get the equilibrium association constant of 43,115 ± 1,383.9 M^{-1} and 33,728 ± 1,274 M^{-1} for fluorescence intensity data and peak area data respectively. The calculated amplitudes for fluorescence intensity and peak area data are 683.5 ± 10.85 and 43,075 ± 756 AU respectively and the resultant Hill coefficients are 1.025 ± 0.031 and 0.917 ± 0.027 respectively. As the Hill coefficients were approximately 1 for both data sets, we refit the data to the Hill equation with a coefficient constrained to 1 indicating non-cooperative or single-site binding. The constrained fit yielded a K_a of 42,704 ± 1,296 M^{-1} and an

amplitude of 69 ± 5 AU for data derived from fluorescent intensity. The constrained fit for peak area data produced a K_a of 35,542 ± 1,171 M^{-1} and an amplitude of 41,084 ± 282. A (K_d) of 23.2 ± 0.7 μM and 30 ± 1 μM were derived from both the fluorescent emissions and the peak area data sets respectively. These values are in fair agreement with each other and reflect a tight/stable binding that is comparable to the binding of ATP and YME1L-AAA+ which was shown to have an experimental dissociation constant of 29.8 ± 3 μM. [21]

We observe that the peak emissions wavelength remains roughly constant at around 350 nm as protein concentration increases (**figure 12.C**). This is consistent with the expected fluorescent trend of tryptophan in the case where the lid domain of YME1L-AAA+ remains largely in an "open" state such that bound vanillin aurone is predominantly interacting with Walker A and P-loop regions on the base domain. Upon hydrogen bonding with the indole of tryptophan, fluorescence emissions will be red shifted and quenched.[21] Without the lid domain closing around the W518 in the NTP binding site, no significant red shift of the peak emission wavelength is expected. Here we observe emission wavelengths that remains constant throughout the course of the titration (**figure 12.C**) indicating that there is no hydrogen bonding with the indole. This observation is consistent with the behavior of tryptophan engaged in pi-pi stacking with vanillin aurone as was predicted (**figure 11**) rather than hydrogen bonding with the vanillin aurone. Because vanillin aurone does not hydrogen bond with the indole nitrogen, the nitrogen remain able to interact with water causing no change in the emission wavelength.

4.4. Binding observed through vanillin aurone fluorescent signal

Because vanillin aurone is itself fluorescent, we designed an experiment to observe the change in vanillin aurone emissions upon aurone binding. While keeping the concentration of vanillin aurone constant at 30 μM we titrated in YME1L-AAA+ and observed emissions of the vanillin aurone when excited at 436 nm. As we have seen, the fluorescence emissions of vanillin aurone increase when in less polar solvent environments. Therefore, it can be predicted that upon binding, the vanillin aurone will be shielded in part from interactions with the polar solvent environment. This shift to an effectively nonpolar local environment along with the stabilization of a planar vanillin aurone structure, the state associated with increased fluorescence intensity, in the bound state is predicted to result in an increase of vanillin aurone fluorescence emissions upon binding to YME1L-AAA+. Indeed, titrations reveal a linear increase in vanillin aurone fluorescent emission intensities and peak area. As shown in **figure 13.A**, fluorescent emissions are also blue shifted toward shorter wavelengths as protein concentration increases. This shift is also described in **figure 13.D** where the peak emission wavelength is plotted as a function of YME1L+AAA+ concentration such that a biphasic trend is observed as the vanillin aurone transitions from a predominately polar environment to a predominantly nonpolar environment. This reflects the decrease in polarity of the local environment around vanillin aurone upon binding to YME1L-AAA+ and is consistent with our initial characterization of vanillin aurone fluorescence.

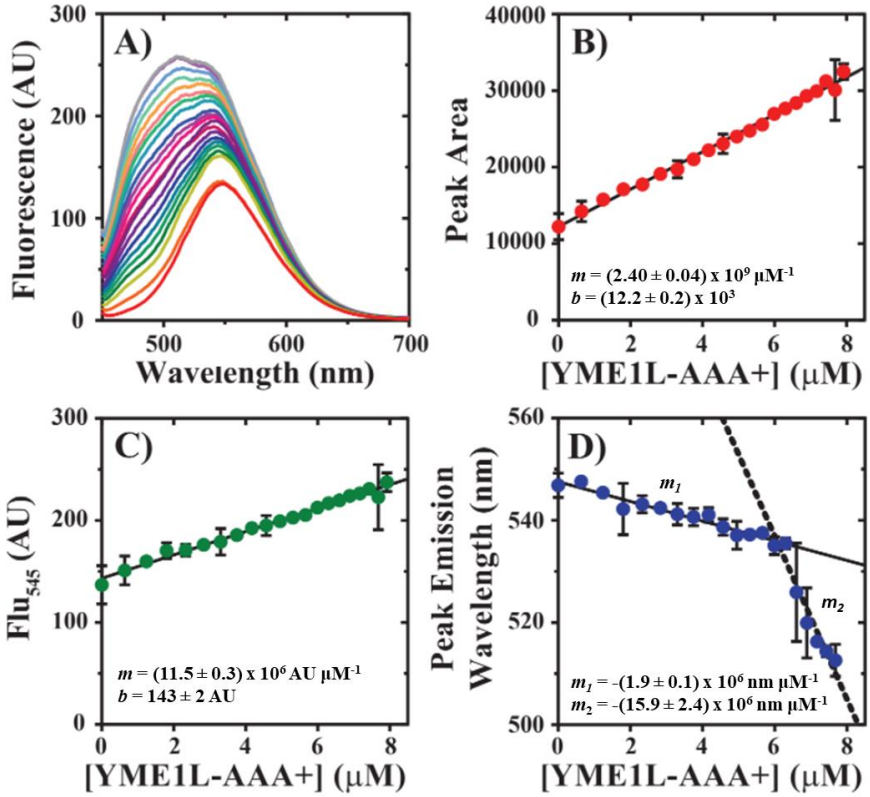

Figure 13: Binding observed through vanillin aurone signal. All data points and spectral lines shown represent an average of data collected in triplicate **A)** The fluorescent spectra of data collected in triplicate where vanillin aurone fluorescence intensity is plotted as a function of wavelength. Each spectral line represents a different concentration of YME1L-AAA+ ranging from 0.64 μM up to 7.9 μM. **B-C)** Peak area and vanillin aurone fluorescent intensity are plotted as a function of increasing YME1L-AAA+ concentration. The straight line is the best fit to a linear least squares analysis and produced the equations printed on the graphs. **D)** Peak emission wavelength is plotted as a function of increasing YME1L-AAA+ concentration. As the data is biphasic, each phase is treated with linear least squares analysis separately and yield the equations as shown on the graph.

Both peak area and fluorescence intensity increase linearly with the continued addition of YME1L-AAA+ (**figures 13.B** and **13.C**) This trend suggests that protein binding may alter vanillin aurone conformation to increase the population of planar state molecules in water, as the planar fluorescent state is more fluorescent than the TICT state. It is necessary to note that this titration was performed at conditions in which the vanillin aurone is in excess for the entirety of the titration such that it would not be expected to observe a plateau in the emission intensity data or peak area data as the protein concentration increases.

5. Cell viability assays

With these data indicating vanillin aurone binding to the AAA+ binding domain of a model AAA+ superfamily protein, we asked if vanillin aurone may prove toxic to cells. If vanillin aurone is able to permeate the cell, it would be highly toxic as a result of binding ATPases which are ubiquitous and structurally homogeneous in the cell. Such an interaction would provide the basis for vanillin aurone development as a potential therapeutic.

To assess cell permeability, we treated HeLa cells with 100 μM vanillin aurone and co-stained the cells with Hoescht, a blue-fluorescent dye that localizes to the nucleus.[21] Fluorescence confocal microscopy was used to image the cells where vanillin aurone was excited at 488 nm and Hoescht was selectively excited at 405 nm. Dye-specific filter sets were used to selectively observe emissions. After treatment, the vanillin aurone, which exhibits green fluorescence, was found to cross the cell membrane as shown by the bright green fluorescence in the cells of **figure 14.A-D**. As can be seen in the second image on the top row, there is some

green fluorescence observed within the nucleus as well. However, rather than assuming that vanillin aurone also permeates the nucleus, we propose that this is bleed through from the co-stain, Hoescht. As a control the experiment was repeated with only vanillin aurone treatment. In those images, we still observe bright green fluorescence within cells, however the fluorescence stays outside the nucleus (**figure S4**).

Figure 14.C shows transmitted light photomultiplier tube (T-PMT) images of the HeLa cells. In these T-PMT images living cells and collapsed dead cells can be observed in the image of the cells that were treated with vanillin aurone. The control, DMSO and Hoescht staining only, does not contain these dense, collapsed cells. The vanillin aurone treated HeLa cells when excited at 488 nm show the same dense, collapsed cells as seen in the T-PMT (**figure 14.A**). These dead cells show up as bright green indicating the presence of vanillin aurone. This observation supports the conclusion that vanillin aurone is toxic to cells which may be due to its AAA+ protein family binding activity. However, future work is needed to conclusively demonstrate this effect in a cellular environment.

To evaluate the cellular response upon vanillin aurone treatment we incubated HeLa cells with vanillin aurone for 24 hours for use in a PrestoBlue™ cell viability assay to assess vanillin aurone toxicity. As **figure 14.B** shows, the cell

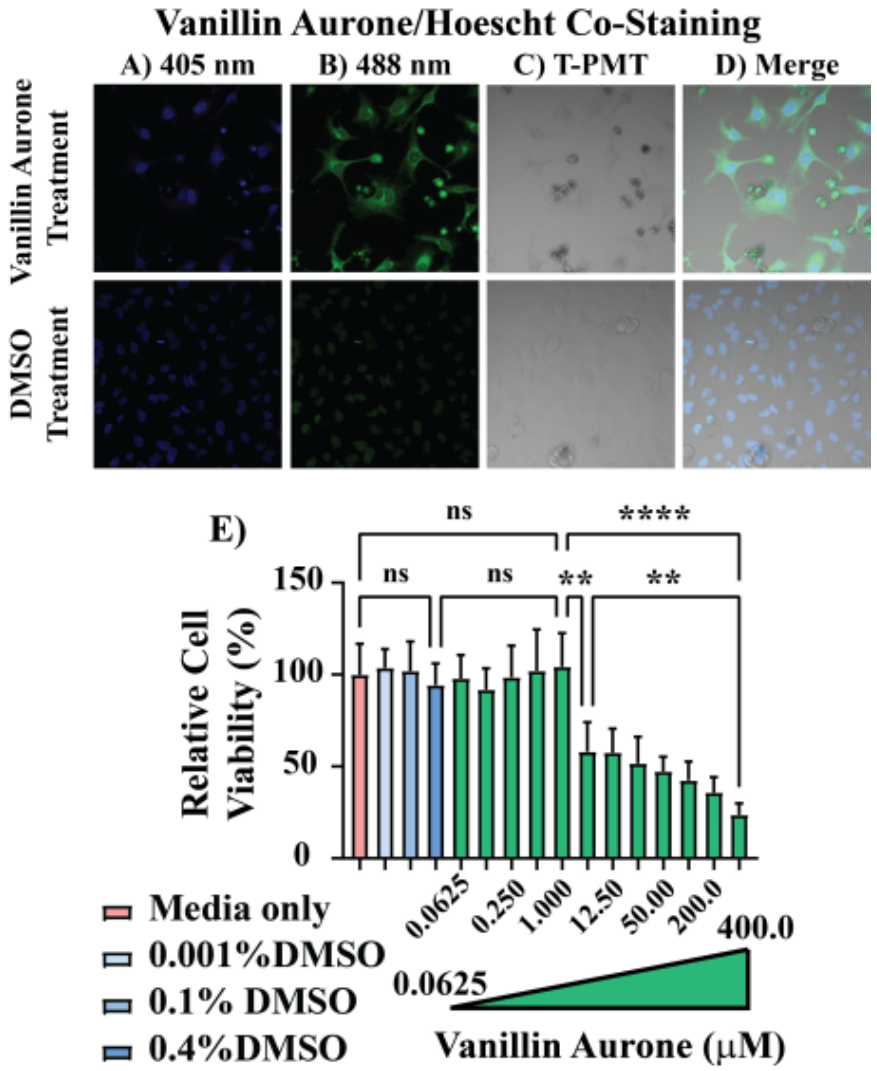

Figure 14: Fluorescent cell images and cell viability assay results. Fluorescent cell images of HeLa cells stained with both vanillin aurone and Hoescht. The control group, treated with only DMSO solvent and Hoescht stain is shown in the second row of images while vanillin aurone and Hoescht duel stained HeLa cell images are shown across the first row. **A)** Fluorescent images of the cells upon excitation of the Hoescht cells at 405 nm. **B)** Fluorescent images of the cells upon selective excitation of vanillin aurone at 488 nm. **C)** Images of the non-fluorescent T-PMT image capturing all present cells. **D)** The fourth column overlays the 405 nm and 488 nm excitation fluorescent images with the T-PMT images for each treatment condition (ie. with or without vanillin aurone). **E)** graphical representation of the PrestoBlue™ cell viability assay. Relative cell viability is shown as a function of increasing vanillin aurone concentration (green). Each bar represents the average of data collected in triplicate. Controls are shown where HeLa cells are treated with only media (pink) and media with a specified composition of DMSO (blue). ANOVA tests were applied to these data such that **ns** = not significant with a $p \geq 0.1234$, ***** represents $p < 0.0332$, ****** represents $p < 0.0021$, ******* represents $p < 0.0002$, and ******** represents $p < 0.0001$

viability decreases as vanillin aurone concentration increases such that an IC50 is reached between 1 - 7 μM. This preliminary work confirms that vanillin aurone indeed causes cell death. This work provides the foundation for the development of vanillin aurone for therapeutic applications.

CHAPTER 3: MATERIALS AND METHODS

1. ***Materials:*** All reagents and solvents, including benzofuran, vanillin, acetone, DMSO, ethanol, and toluene were commercially obtained to be greater than 95% purity. Solvents used are ACS grade; no specific measures were taken to ensure the solvents were anhydrous. Double distilled water from an Elga Pure Lab Ultra water filtration system was used for all aqueous solutions and assays. All fluorescence data was collected on a Hitachi F-4500 fluorescence spectrophotometer. Absorbance values were collected on a Hitachi U-2900 spectrophotometer.
2. ***Methods***

2.1. Vanillin aurone synthesis

The vanillin aurone is synthesized through an acid catalyzed aldol condensation reaction. Benzofuranone is added to vanillin in glacial acetic acid with catalytic HCl and the reaction is mixed for roughly 2-3 hours. Cross aldol reactions can result in excess byproduct formation if the ketone or aldehyde engage in a self-Aldol reaction.[22] However, the selection of an aldehyde not capable of enol formation, such as vanillin, and a ketone that is able to form an enol helps to direct the reaction toward the desired product. It is also helpful that vanillin is an

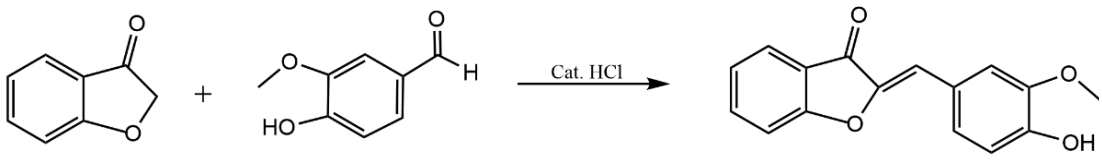

Figure 15: Synthetic scheme of vanillin aurone

aldehyde and for steric reasons is more reactive than benzofuranone. This will further encourage the cross-Aldol reaction over the self-Aldol.[25]

After three hours, the homogenous mixture is diluted with roughly 10 mL of water resulting in a precipitate, the vanillin aurone, that is filtered then washed with additional water. Finally, the precipitate is air dried and then further dried in a desiccator overnight. The product is obtained in 75-90% yield depending on scale and is pure by 1H NMR.

2.2. Fluorescence titrations

Solid vanillin aurone was weighed and dissolved in dimethyl sulfoxide (DMSO) to make a 1 mM stock solution. The stock solution was made by using the known molecular weight of vanillin aurone, 268.27 g/mol. Using the 1 mM stock solution, a 100 μM solution was made using each of five solvents: toluene, acetone, DMSO, ethanol, and water. The 100 μM solutions served as the titrant for the fluorescent titration experiments. For each condition, the optimal excitation wavelength was determined by conducting an emission scan on the 100 μM vanillin aurone titrant solution. The optimal excitation wavelength varied slightly with the

change in solvent environment. The excitation wavelengths and emission wavelength ranges for vanillin aurone in each solvent are as follows: acetone, 418 nm, 430-700 nm; toluene, 423 nm, 450-700 nm; DMSO, 421 nm, 430-700 nm; H_2O, 436 nm, 445-700 nm; ethanol, 425 nm, 450-700 nm. The observed maximum fluorescent emissions wavelengths for the toluene, acetone, DMSO, ethanol, and water conditions are 491, 499, 514, 516, and 539 nm respectively.

Following the collection of a blank conducted on 300 μL of pure solvent, two microliters of titrant was added and followed by excitation and collection of fluorescent emissions. This process was repeated adding two microliters at a time until a total addition volume of 50 μL was reached. Once a total titrant addition volume of 50 μL was reached the titrant increment was increased from two microliters to ten microliters at a time until a total addition volume of 200 μL was reached. Data was collected in this way in triplicate for each of the five solvent conditions and then analyzed in Excel software.

2.3. Extinction coefficient calculations

To determine the extinction coefficient (ε) for vanillin aurone in each of the solvent conditions, a series of five solutions of increasing vanillin aurone concentrations were made. For the DMSO solvent condition, solid vanillin aurone was dissolved into DMSO in order to make a 1 mM stock solution. This stock solution was then further diluted into more DMSO to make 5, 10, 15, 20, and 25 micromolar solutions. Each of these five solutions was placed in a clean quartz cuvette and a Hitachi U-2900 spectrophotometer was used to measure the absorbance of the vanillin aurone in DMSO at that concentration. Absorbance

values were recorded for each of the five concentrations then plotted as a function of vanillin aurone concentration. According to the Beer-Lambert law ($\mathbf{A} = \mathbf{bc}\varepsilon$, where **A** is the chromophore absorbance, **b** is path length, **c** is the chromophore concentration, and ε is the molar absorptivity or extinction coefficient), when absorbance is plotted as a function of chromophore concentration the relationship will be linear and can be fit to a straight line having a slope equivalent to the extinction coefficient for that chromophore in that particular solvent environment.[16] Extinction coefficients were calculated in this way for vanillin aurone in each of the solvents and the excitation wavelengths used were the optimal wavelengths previously determined for the fluorescence titration experiments. No special efforts were taken to ensure solvents were dry, therefore these solvents may have contaminating water present.

Due to limited solubility in water, calculation of the ε for vanillin in water deviated slightly from the described procedure. Instead of dissolving solid vanillin aurone directly into water to make the stock solution, the 1 mM DMSO stock was used and diluted into pure water to make the five small concentrations needed to obtain absorbance values.

2.4. Density functional theory calculations

The geometry of vanillin aurone was optimized in each solvent using density functional theory (DFT) with the B3LYP functional and 6-31+G* basis set. [26,27] The conductor-like polarizable continuum model (C-PCM) was used to describe the solvent effect on the geometry. [28-30] The dielectric constant and optical

dielectric for each solvent was obtained from the Minnesota solvent descriptor database.[31]

Vertical electronic excitation energies (VEEs) were computed with time-dependent DFT (TD-DFT) using the B3LYP/6-31+G* functional and basis set in each solvent. The random phase approximation (RPA) was used for TD-DFT. [32] The C-PCM solvation model was also used for TD-DFT, although the non-equilibrium linear response formalism was used to account for the effect of solvation on the excitations.[33] It is assumed that the VEEs are a good approximation for the wavelength of maximal absorbance (i.e., that the Franck-Condon approximation holds for this system).

Fluorescence wavelengths were computed as VEEs after optimizing the fluorescent (excited-state) geometry. The same TD-DFT protocol is used for computing the fluorescence energies, including the use of RPA. However, the excited-state geometry optimizations were performed using the Tamm-Dancoff approximation instead of RPA.[34]

The fluorescence calculations were performed for three types of fluorescent states: one where the aurone is initially in a planar configuration, which resulted in the optimization of a planar fluorescent state, one where the aurone was initially twisted around the exocyclic single bond, which led to optimization of a twisted intramolecular charge transfer (TICT) state, and one where the aurone is deprotonated at the phenol group.

All calculations in this work were performed with the Q-Chem 5.4.0 electronic structure software package. [29,33]

2.5. Molecular dynamics vanillin aurone docking

Model Preparation: The *Swiss-Model* web server was used to construct a human YME1L-AAA+ domain homology model against a reference structure of the resolved yeast YME1 (PDB code 6az0). Vanillin models were constructed in Avogadro and subsequently docked with Autodock Vina to YME1L-AAA+ coordinates known to participate in nucleotide binding. Docked poses were then validated with all-atom molecular dynamics (MD) in Gromacs.

MD: The *Swiss-Param* web server and *pdb2gmx* were used to generate Charmm36 compatible parameter sets for vanillin and YME1L-AAA+, respectively. The docked complex was solvated in a rhobmic dodecahedron with TIP3P water. Neutralizing ions were added and the system was minimized by steepest descent for 1000 steps. Heavy atoms were then restrained during a brief 100 ps simulation via a canonical ensemble (NVT) with velocity rescaling to bring the system temperature to 298.15 K. To encourage a stable ligand interaction, the restraining potential was relaxed by slowly reducing the applied force constant (k) from 1000 to 250 kJ mol^{-1} nm^2 throughout successive rounds of additional equilibration in accordance with the isothermal-isobaric ensemble (NPT). Temperature and pressure were maintained at 298.15 K and 1.0 bar with velocity rescaling and Berendsen pressure coupling, respectively.[35] Restraints were then removed, and production MD was allowed to proceed for 200 ns. The NPT ensemble was maintained during production MD by Nose-Hoover and Parinello-Rahman temperature and pressure coupling, respectively. [36-38] Dynamic equilibration was

assessed by RMSD block averaging, with equilibrated frames used for subsequent analysis of binding site interactions.

2.6. Fluorescent titrations with YME1L-AAA+

All titrations were carried out using a Hitachi F-4500 fluorescence spectrophotometer and executed in triplicate.

2.6.1. Titration Design 1: YME1L-AAA+ titrant and vanillin aurone fluorescence observed

YME1L-AAA+ was expressed and purified as previously described by the Miller Lab Group.[21] Purity was assessed to be greater than 95% by Coomassie staining methods. The protein was then dialyzed into a buffer consisting of 10% glycerol, 25 mM HEPES, and 150 mM NaCl using Thermo Scientific Slide-A-Lyzer® 20,000 MWCO MINI dialysis units. After dialysis, the protein concentration was determined by taking the average of absorption readings taken by a nanodrop spectrophotometer and calculating the concentration by using the Beer-Lambert equation in combination with the known ε for YME1L-AAA+, 1.15 x 10^4 $M^{-1}c^{-1}$ at 280 nm. This protein solution at 19.81 μM was used as the titrant for this set of experiments.

For the experiment, a 300 μL, 30 μM solution of vanillin aurone was prepared by diluting the previously described 1 mM vanillin aurone stock in DMSO into YME1L-AAA+ dialysate. This solution was placed in a The titration was conducted by adding 10 μL of protein titrant to the vanillin aurone solution in the cuvette, then allowing four minutes of equilibration time before exciting the vanillin aurone at 436 nm and collecting fluorescence emissions from 445 nm –

700 nm. Slit widths of 5.0 nm and PMT voltage of 700 V were used. quartz fluorescence cuvette and used for the fluorescent titration experiment. This process was repeated at 10 uL increments until a total addition volume of 200 µL was reached. Data from this experiment was analyzed in Excel where dilution of the vanillin aurone as YME1L-AAA+ concentration increased was adjusted for.

2.6.2. *Titration Design 2: Vanillin aurone titrant and YME1L-AAA+ W518 fluorescence observed*

YME1L-AAA+ was expressed, purified and dialyzed as previously described.[21] This protein was used to make a 2.97 µM solution which was placed in a quartz fluorescence cuvette for the titration experiment. The titrant was prepared from the 1 mM vanillin aurone in DMSO stock solution as before and diluted into YME1L-AAA+ dialysate to a 500 µM solution.

The titrant was added to the 2.97 µM YME1L-AAA+ solution in 10 uL increments. This mixture was allowed four minutes to equilibrate before exciting the W518 in YME1L-AAA+ at 295 nm and observing emissions from 305 nm – 400 nm. Slit widths of 5.0 nm and a PMT voltage of 700 V were used. The data was then corrected for dilution of the tryptophan concentration and analyzed with Excel software.

2.7. Fluorescent cell imaging and cell viability assay

HeLa S3 cells were purchased from ATCC (CCL2.2) and cultured in Roswell Park Memorial Institute 1640 medium (Gibco; 11875093) supplemented with 10% (v/v) fetal bovine serum and 100U/mL penicillin and streptomycin cocktail (Gibco; 15140122, RPMI complete medium), incubated at 37°C in 5% CO_2, and

passaged every 3-5 days using trypsin-EDTA (Gibco 25200056). Prior to treatment, HeLa cells were seeded using a concentration of $1x10^5$ cells/mL in 35mm Cellvis dishes with a 14mm #1.5 glass coverslip bottom (Fisher Scientific; NC0794151) and allowed to attach for 16-18 hours (overnight). The cells were then washed in prewarmed 1x phosphate buffered saline (PBS) pH 7.4 without calcium or magnesium (Gibco10010023) and treated with 100µM Vanillin aurone in RPMI complete medium (with 0.1% [v/v] DMSO as a cosolvent), or RPMI with 0.1% (v/v) DMSO as a control, for 24 hrs. Fluorescent cell imaging was conducted using a Zeiss LSM 700 confocal microscope. HeLa cells treated with vanillin only or DMSO control were excited using a 405 nm laser detecting wavelengths above 493 nm (gain=525). In cells costained with Hoescht 33342, NucBlue live reagent from the Invitrogen ReadyProbes cell viability imaging kit (Hoechst; Fisher Scientific; R37610) was added at least 15 minutes prior to the completion of the 24 hour imaging according to the manufacturer's protocol. For imaging experiments, HeLa cells with vanillin with Hoechst, or controls were excited using a 405 nm laser detecting wavelengths of light below 475 nm (Hoechst; gain=550) or at wavelengths above 502 nm (vanillin; gain=600). To account for the cross-talk between the two fluorophores HeLa cells with vanillin only (or DMSO control) were taken using the same settings at a later date. Although cross-talk was occurring as shown by the images, HeLa cells imaged using the Hoechst filter settings and treated with the vanillin only were remarkably dimmer than those treated with both Hoechst and vanillin, therefor the brightness of both the vanillin only treated cells, and their DMSO control, was increased evenly for both filter

settings for both experiments for visual clarity. This disparity between the vanillin aurone+Hoechst and the vanillin only treatments could be due to a loss of fluorescence from multiple freeze thaw cycles, or due to potential FRET activity increasing or shifting the fluorescence of the vanillin in the presence of Hoechst. Further experimentation is warranted.

To assess the toxicity of vanillin aurone a PrestoBlue™ cell viability assay was conducted. $1x10^4$ cells per well were seeded in a clear 96 well flat-bottom tissue culture plate and allowed to attach overnight. The cells were then washed with 1x PBS and treated the vanillin aurone in RPMI complete medium at the concentrations as shown in **figure 14.e** and incubated as mentioned earlier for 24 hours. The cells were then washed with 1x PBS, and 100 µL 1x PrestoBlue™ reagent in RPMI complete medium was added to the cells for 1hr according to the manufacturer's protocol. The 570 nm absorbance for each well was determined using the CLARIOstar microplate reader and absorbance for 600 nm was subtracted as a reference wavelength ($abs_{570\ nm}$ - $abs_{600\ nm}$) following the manufacturer's protocol. HeLa cells treated with media only, or with 0.4 %, 0.1 %, or 0.001 % DMSO, were also included for each replicate as controls. Each treatment was performed as three wells over three different biological replicates, $n=9$. The data was standardized for each replicate as a percent of the untreated average difference of $abs_{570\ nm}$ - $abs_{600\ nm}$. The difference of $abs_{570\ nm}$ - $abs_{600\ nm}$ from 3 wells per replicate containing only 1x PrestoBlue™ in RPMI without cells was subtracted from each measurement as a blank. Statistical significance was determined using a parametric 1-way Brown-Forsythe and Welch's ANOVA with a

Dunnet's T3 correction. **p<0.01, ***p<0.001, ****p<0.0001. Only comparisons between each concentration and the untreated control as well as the comparison between 1 μM and 6.25 μM are shown.

CHAPTER 4: CONCLUSIONS

Our data reports the synthesis and characterization of a fluorescent aurone dye named the vanillin aurone for the vanillin substituent attached to the benzofuran ring. We show that this fluorophore excites around 420 nm and is highly solvent sensitive displaying much increased fluorescent intensity and blue shifted spectra as solvent polarity decreases. The solvatochromic behavior appears to arise from some variance in the emissions process as the ε remains relatively consistent across solvent environments. However, TD-DFT calculations identified three likely fluorescent states which display distinct emissions patterns that may suggest different quantum yield values for each state. The planar and deprotonated states contribute more positively to the observed fluorescence intensities while the TICT state detracts from overall fluorescent intensity. The calculated data in comparison with the experimental data suggest that the vanillin aurone exists in a heterogeneous mixture of the three fluorescent states with polar environments causing the aurone to favor the less fluorescent TICT state. More work will be needed to understand the solvent-fluorophore interactions that drive the adoption of one fluorescent state over another. It may also be clarifying to evaluate the effect

of pH manipulation on fluorescence intensities, as it is predicted that the brightest fluorescent state is the deprotonated state.

As the vanillin aurone structure resembles that of nucleoside triphosphates we used the model protein YME1L-AAA+ to assess the potential for AAA+ domain binding. We found that YME1L-AAA+ does indeed bind vanillin aurone with a K_d of roughly 25 μM, where the reported K_d for the protein's natural substrate, ATP is 25.8 ± 4.9 μM.[20] This binding was observed and quantified by tryptophan dependent fluorescent titrations as well as vanillin aurone dependent fluorescent titration. Because ATPases can be found in large numbers throughout cells, a dye that competitively binds ATPases would be expected to be highly toxic. A PrestoBlue™ cell viability assay was conducted to evaluate vanillin aurone toxicity. Vanillin aurone treatment was found to be toxic to HeLa cells between 1 and 7 μM, although future work is needed to determine the IC50 more specifically. These data shows consistent binding of vanillin aurone to ATPases combined with toxicity data provides a starting point for future development of the aurone as a therapeutic agent.

References

[1] Kricka, L. J.; Fortina, P. Analytical Ancestry: “Firsts” in Fluorescent Labeling of Nucleosides, Nucleotides, and Nucleic Acids. *Clinical Chemistry* **2009**, *55* (4), 670–683.

[2] Donaldson, L.; Williams, N. Imaging and Spectroscopy of Natural Fluorophores in Pine Needles. *Plants* **2018**, *7* (1), 10.

[3] Keshri, S. K.; Mandal, K.; Kumar, Y.; Yadav, D.; Mukhopadhyay, P. Naphthalenediimides with High Fluorescence Quantum Yield: Bright-Red, Stable, and Responsive Fluorescent Dyes. *Chemistry – A European Journal* **2021**, *27* (23), 6954–6962.

[4] Mahato, R. Multifunctional Micro- and Nanoparticles. *Emerging Nanotechnologies for Diagnostics, Drug Delivery and Medical Devices* **2017**, 21–43.

[5] Lakowicz, J. R. *Principles of fluorescence spectroscopy*; Springer: New York, NY, 2010.

[6] Experimental Methods in Polymer Science. *Polymers, Interfaces and Biomaterials* **2000**.

[7] Boumendjel, A. [General Articles] Aurones: A Subclass of Flavones with Promising Biological Potential. *Current Medicinal Chemistry* **2003**, *10* (23), 2621–2630.

[8] Chien, S.-C.; Chiu, H.-L.; Cheng, W.-Y.; Hong, Y.-H.; Wang, S.-Y.; Wu, J.-H.; Shih, C.-C.; Liao, J.-C.; Kuo, Y.-H. Pterocarpans from *Derris Laxiflora*. *Natural Product Communications* **2016**, *11* (1).

[9] Mazziotti, I.; Petrarolo, G.; La Motta, C. Aurones: A Golden Resource for Active Compounds. *Molecules* **2021**, *27* (1), 2.

[10] Roussaki, M.; Costa Lima, S.; Kypreou, A.-M.; Kefalas, P.; Cordeiro da Silva, A.; Detsi, A. Aurones: A Promising Heterocyclic Scaffold for the Development of Potent Antileishmanial Agents. *International Journal of Medicinal Chemistry* **2012**, *2012*, 1–8.

[11] Espinosa-Bustos, C.; Cortés-Arriagada, D.; Soto-Arriaza, M. A.; Robinson-Duggon, J.; Pizarro, N.; Cabrera, A. R.; Fuentealba, D.; Salas, C. O. Fluorescence Properties of Aurone Derivatives: An Experimental and Theoretical Study with Some Preliminary Biological Applications. *Photochemical & Photobiological Sciences* **2017**, *16* (8), 1268–1276.

[12] Shanker, N.; Dilek, O.; Mukherjee, K.; McGee, D. W.; Bane, S. L. Aurones: Small Molecule Visible Range Fluorescent Probes Suitable for Biomacromolecules. *Journal of Fluorescence* **2011**, *21* (6), 2173–2184.

[13] Schmitt, J.; Handy, S. T. A Golden Opportunity: Benzofuranone Modifications of Aurones and Their Influence on Optical Properties, Toxicity, and Potential as Dyes. *Beilstein Journal of Organic Chemistry* **2019**, *15*, 1781–1785.

[14] Reichardt, C. *Solvents and solvent effects in organic chemistry. 2., rev., ENL. Ed. (repr.)*; VCH XXII: Weinheim - Basel etc, 1990.

[15] Su, Y.; Li, K.; Yu, X. Theoretical Studies on the Fluorescence Enhancement of Benzaldehydes by Intermolecular Hydrogen Bonding. *The Journal of Physical Chemistry B* **2019**, *123* (4), 884–890.

[16] Clark, J. The beer-lambert law. https://chem.libretexts.org/Bookshelves/Physical_and_Theoretical_Chemistry_Textbook_Maps/Supplemental_Modules_(Physical_and_Theoretical_Chemistry)/Spectrosc

opy/Electronic_Spectroscopy/Electronic_Spectroscopy_Basics/The_Beer-Lambert_Law (accessed Mar 30, 2022).

[17] Wehry, E. L.; Rogers, L. B. Application of Linear Free Energy Relations to Electronically Excited States of Monosubstituted Phenols. *Journal of the American Chemical Society* **1965**, *87* (19), 4234–4238. https://doi.org/10.1021/ja00947a003.

[18] Iino, R.; Kinbara, K.; Bryant, Z. Introduction: Molecular Motors. *Chemical Reviews* **2020**, *120* (1), 1–4.

[19] Miller, J. M.; Enemark, E. J. Fundamental Characteristics of AAA+ Protein Family Structure and Function. *Archaea* **2016**, *2016*, 1–12.

[20] Chang, C.-W.; Lee, S.; Tsai, F. T. Structural Elements Regulating AAA+ Protein Quality Control Machines. *Frontiers in Molecular Biosciences* **2017**, *4*.

[21] Miller, J. M.; Brambley, C. A.; Marsee, J. D. Examination of the Role of Mg2+ in the Mechanism of Nucleotide Binding to the Monomeric YME1L AAA+ Domain. *Biochemistry* **2020**, *59* (45), 4303–4320.

[22] Hill, A. Proceedings of the Physiological Society: January 22, 1910. *The Journal of Physiology* **1910**, *40* (suppl), iv-vii.

[23] Latt, S. A.; Stetten, G.; Juergens, L. A.; Willard, H. F.; Scher, C. D. Recent Developments in the Detection of Deoxyribonucleic Acid Synthesis by 33258 Hoechst Fluorescence. *Journal of Histochemistry & Cytochemistry* **1975**, *23* (7), 493–505.

[24] Smith, J. G. *Organic Chemistry*, 2nd ed.; McGraw-Hill Higher Education: Boston, MA, 2008.

[25] Ashenhurst, J. The acid-catalyzed aldol reaction. https://www.masterorganicchemistry.com/2010/06/02/the-acid-catalyzed-aldol-reaction/ (accessed Mar 27, 2022).

[26] Becke, A. D., Density-Functional Exchange-Energy Approximation with Correct Asymptotic Behavior. *Phys. Rev. A* **1988,** *38* (6), 3098.

[27] Lee, C.; Yang, W.; Parr, R. G., Development of the Colle-Salvetti Correlation-Energy Formula into a Functional of the Electron Density. *Phys. Rev. B* **1988,** *37* (2), 785.

[28] Truong, T. N.; Stefanovich, E. V., A New Method for Incorporating Solvent Effect into the Classical, Ab Initio Molecular Orbital and Density Functional Theory Frameworks for Arbitrary Shape Cavity. *Chem. Phys. Lett.* **1995,** *240* (4), 253-260.

[29] Barone, V.; Cossi, M., Quantum Calculation of Molecular Energies and Energy Gradients in Solution by a Conductor Solvent Model. *J. Phys. Chem. A* **1998,** *102* (11), 1995-2001.

[30] Cossi, M.; Rega, N.; Scalmani, G.; Barone, V., Energies, Structures, and Electronic Properties of Molecules in Solution with the C-Pcm Solvation Model. *Journal of computational chemistry* **2003,** *24* (6), 669-681.

[31] Winget, P.; Dolney, D. M.; Giesen, D. J.; Cramer, C. J.; Truhlar, D. G., Minnesota Solvent Descriptor Database. *Minneapolis, MN: Department of Chemistry and Supercomputer Institute* **1999**.

[32] Bouman, T. D.; Hansen, A. E.; Voigt, B.; Rettrup, S., Large-Scale Rpa Calculations of Chiroptical Properties of Organic Molecules: Program Rpac. *Int. J. Quantum Chem.* **1983,** *23* (2), 595-611.

[33] Cossi, M.; Barone, V., Time-Dependent Density Functional Theory for Molecules in Liquid Solutions. *J. Chem. Phys.* **2001,** *115* (10), 4708-4717.

[34] Hirata, S.; Head-Gordon, M., Time-Dependent Density Functional Theory within the Tamm–Dancoff Approximation. *Chem. Phys. Lett.* **1999,** *314* (3-4), 291-299.

[35] Berendsen, H. J.; Postma, J. P.; van Gunsteren, W. F.; DiNola, A.; Haak, J. R. Molecular Dynamics with Coupling to an External Bath. *The Journal of Chemical Physics* **1984**, *81* (8), 3684–3690.

[36] Parrinello, M.; Rahman, A. Polymorphic Transitions in Single Crystals: A New Molecular Dynamics Method. *Journal of Applied Physics* **1981**, *52* (12), 7182–7190.

[37] Nosé, S. A Unified Formulation of the Constant Temperature Molecular Dynamics Methods. *The Journal of Chemical Physics* **1984**, *81* (1), 511–519.

[38] Hoover, W. G. Canonical Dynamics: Equilibrium Phase-Space Distributions. *Physical Review A* **1985**, *31* (3), 1695–1697.

APENDIX

Supplemental Figures

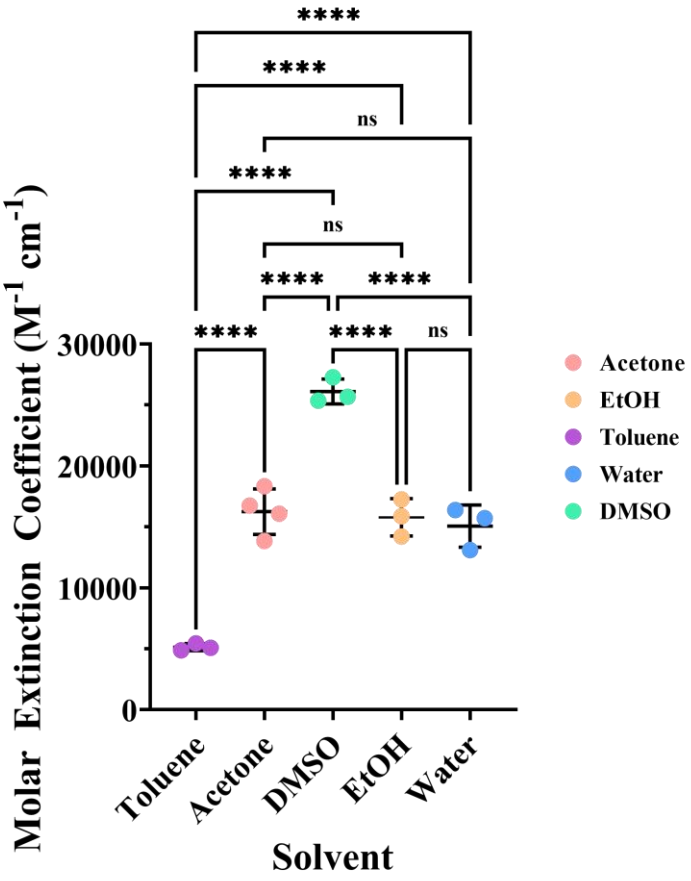

Figure S1: One way ANOVA of vanillin aurone extinction coefficients. Each point on the graph represents a experimentally determined ε for vanillin aurone in the solvent specified by the colored legend. The data was treated with one way ANOVA analysis and pairwise comparisons are included above the data points to indicated significant variance. **ns** indicates $p > 0.1234$ and ******** indicates $p < 0.0001$

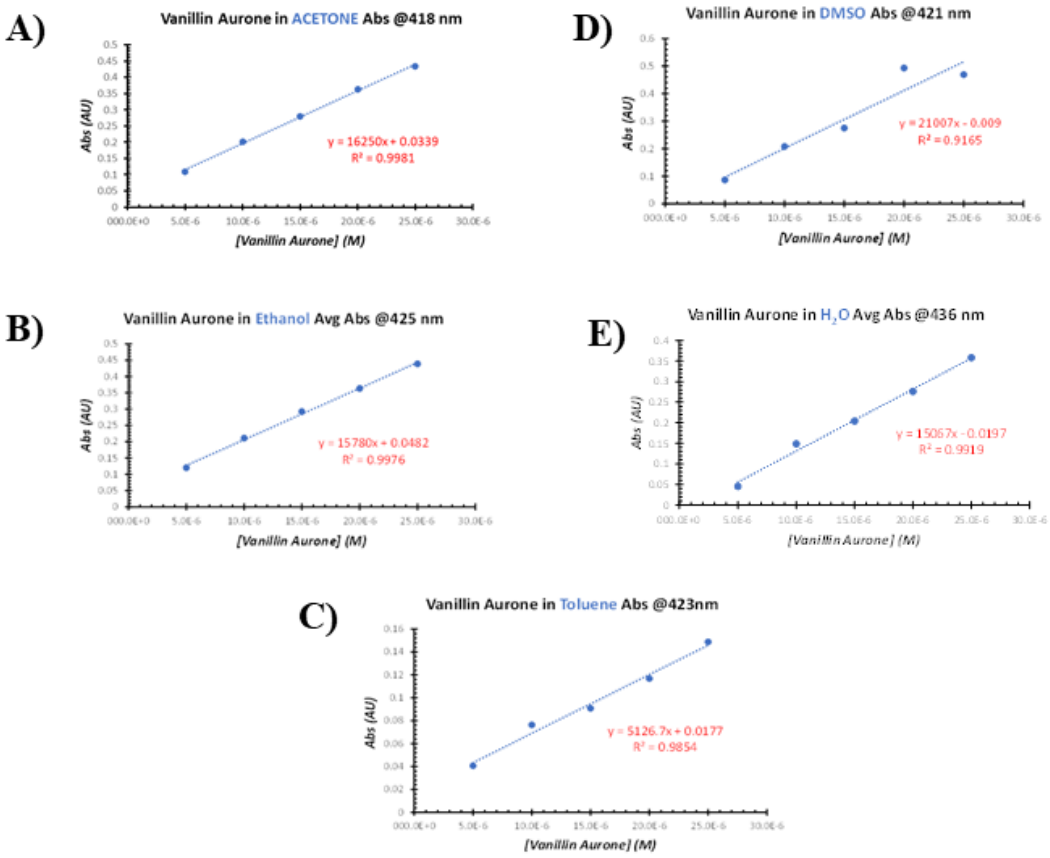

Figure S2: Extinction coefficient calculations All data points are averages of values collected in triplicate. Each data set is fit to a line with the form of y = mx + b and the resultant equations and r^2 values are as printed on each graph. According to the Beer-Lambert law, where A = bcε, the slope of each line is the extinction coefficient (ε) for vanillin aurone in the specified solvent.[16]

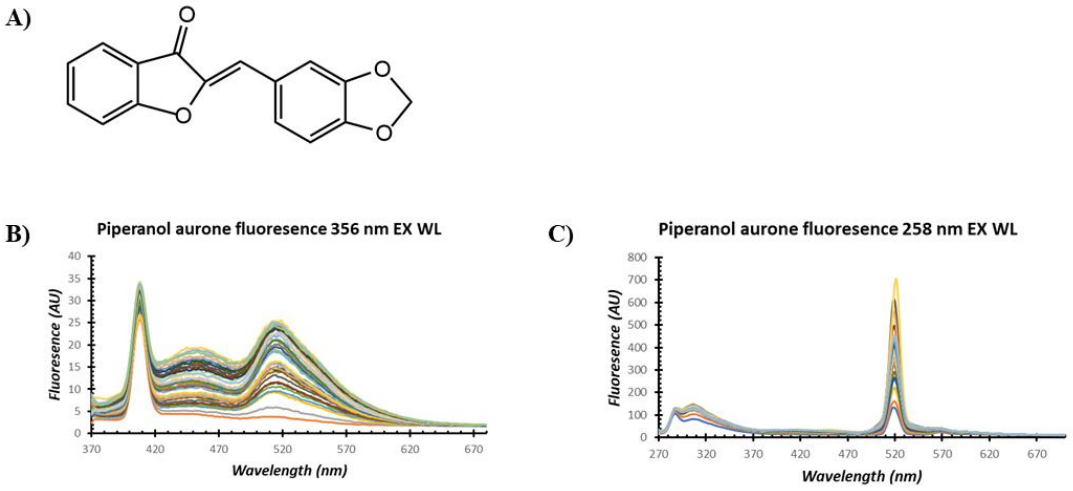

Figure S3: Fluorescent emissions of piperanol aurone in H_2O. A) The chemical structure of the piperanol aurone is depicted where the benzylidene ring of a general aurone structure has been replaced with piperanol. **B-C)** Because two peaks were observed in the excitation scan of piperanol aurone, both fluorescent spectra of piperanol aurone when excited at 258 and 356 nm is shown. The excitation wavelength used is specified in the title of each graph and fluorescence is plotted as a function of wavelength. Each line of the spectra represents a different piperanol aurone concentration ranging from 0.66 μM up to 40 μM.

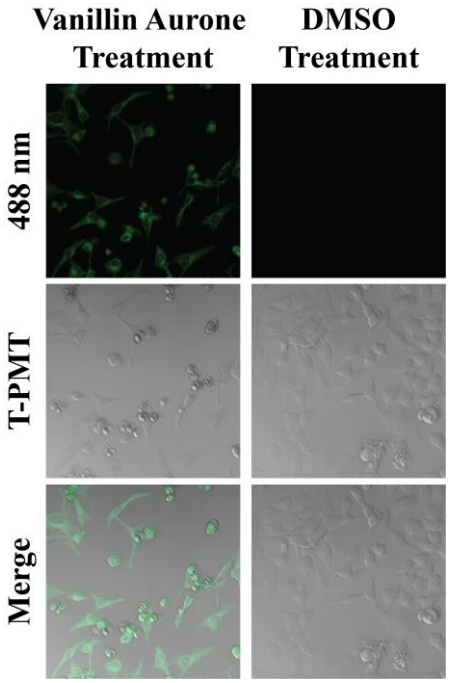

Figure S4: HeLa cell fluorescent images when treated with vanillin aurone alone. HeLa cells that were treated with 100 μM vanillin aurone in DMSO were imaged along side cells treated with DMSO only. Images in the top row show cells that have been excited at 488 nm to excite vanillin aurone present in the cells. The middle row shows the same cells imaged with T-PMT so that all present cells are visible. The bottom row of images merges the first two rows together so that the vanillin aurone can be clearly seen localizing within HeLa cells, however, avoiding the nucleus of the cells.

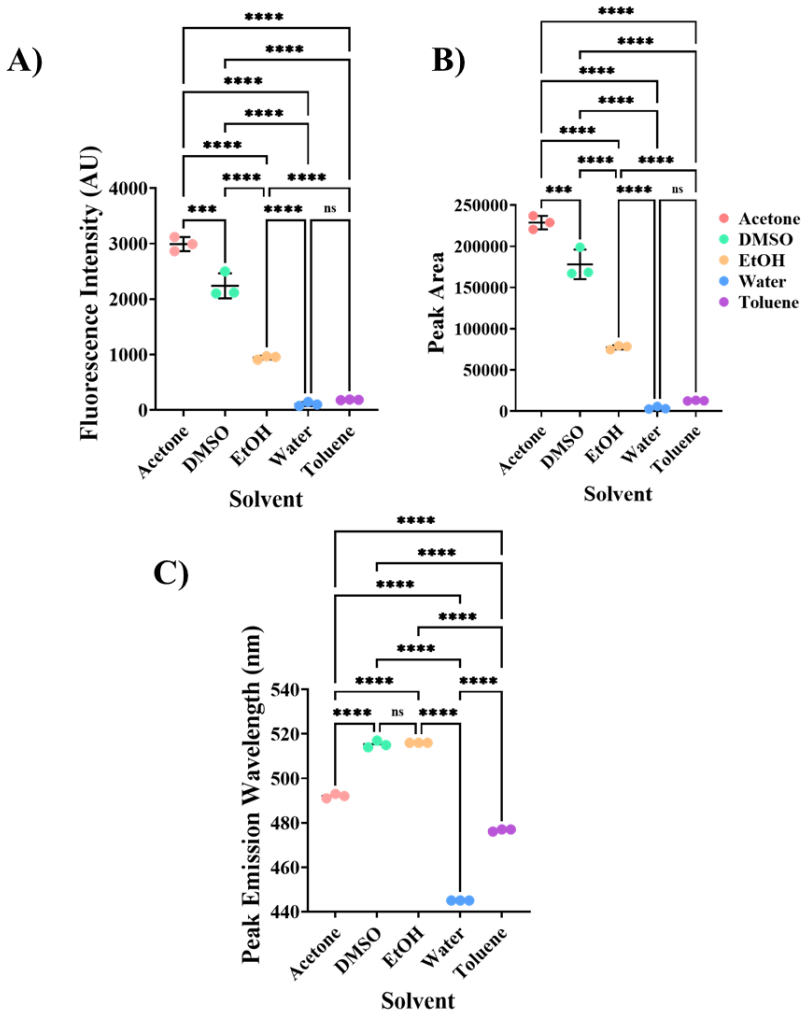

Figure S5: Fluorescence intensity, peak area, and peak emission wavelength vs. polarity index ANOVA This figure analysis the data shown in figure 5. **ns** $p > 0.1234$, ********$p < 0.0001$, *******$p < 0.0002$, ******$p < 0.0021$, *****$p < 0.0332$ **A)** Pairwise one way ANOVA comparisons of the fluorescent intensity of vanillin aurone in each of the five solvent environments specified by colored legend. **B)** Pairwise one way ANOVA comparisons of the peak area, or area under the curve, of vanillin aurone in each of the five solvent environments **C)** Pairwise one way ANOVA comparisons of the peak emission wavelength of vanillin aurone in each of the five solvent environments.